Residual Stresses in Wires: Influence of Wire Length

J. Ruiz, J.M. Atienza, and M. Elices

(Submitted 8 April 2003)

Residual stresses are one of the causes of failures in structural components. These stresses may arise in the fabrication process from many causes. They cannot be easily accounted for because they are both difficult to predict and to measure. X-ray diffraction (XRD) is nowadays a widespread technique for measuring surface residual stresses in crystalline materials. Very small specimens are often used for this purpose due to geometrical restrictions of either the diffractometer sample holder or the component to be inspected. However, the cutting process itself may affect the residual stress state in these specimens, so measured stresses could be misleading. In this work, the influence of specimen length on residual stresses was investigated in cold-drawn ferritic and pearlitic steel wires by XRD measurements and finite element simulations. In the ferritic wires, numerical simulations coincide with experimentally measured stresses. However, in the pearlitic wires the effect of the stresses in cementite (which could not be measured by XRD) has to be taken into account to explain the observed behavior. The results obtained have shown that in both materials the cutting process affects residual stresses, so it is recommended that specimens larger than five times the wire diameter be used.

Keywords cold-drawing, numerical simulation, residual stress, steel wire, x-ray diffraction

1. Introduction

Residual stresses are one of the causes of failures in structural components. It has been reported that failures due to stress corrosion, fatigue, and corrosion-fatigue have been triggered, in most cases, by the presence of high tensile residual stresses.[1-9]

Residual stresses are self-equilibrating internal stresses existing in a free body that has no external forces or constraints acting on its boundary. These stresses may be generated in the fabrication process, in additional heat treatments, or just during the mechanical loading of a component in use.[10] As they are not the result of external loads, they are not "visible"; only their consequences are observed. Therefore, they are often ignored in the design or quality control of a component. This is the reason residual stresses need to be carefully measured, especially in components designed for high-risk applications.

From the various methods devised for the measurement of residual stresses, x-ray diffraction (XRD) appears the most useful to assess surface residual stresses in crystalline materials.[10-18] In this method, the change in the interplanar lattice spacing with respect to the "stress-free" value is used to calculate the strain, from which the stress is derived. However, the interpretation of these measurements is often far from straightforward, especially when small specimens must be used. This may be the case when only a small coupon can be cut from the component to be inspected. In addition to that, in many x-ray diffractometers used for residual stress measurement, the sample holder is designed for very small specimens (typically less that 2 cm in length). The cutting process may affect the residual stress state in these specimens, so measured stresses in the vicinity of free surfaces could be misleading.

In this work, the influence of specimen length on residual stresses was investigated with the aim of determining the minimum size required to obtain realistic values. To this end, longitudinal residual stresses at the surface of two cold-drawn steel wires (with ferritic and pearlitic microstructure) were numerically calculated by the finite element method (FEM) and experimentally measured by XRD.

J. Ruiz, J.M. Atienza, and **M. Elices,** Departamento de Ciencia de Materiales, Universidad Politécnica de Madrid, E.T.S.I. Caminos, Profesor Aranguren s/n. E-28040 Madrid, Spain. Contact e-mail: jr@mater.upm.es.

2. Experimental Procedure

2.1 Material: Wires With Residual Stresses

Straight bars (20 mm diameter and 6 m length) of ferritic and pearlitic steel were specially fabricated by Saarstahl AG (Völklingen, Germany) for this research. The bars were produced by hot rolling and aged to reduce residual stresses to a minimum. Chemical composition of both materials is shown in Table 1.

Conventional tensile tests were performed with a universal testing machine to obtain the mechanical properties of the wires before drawing. The results (average of at least three tests) are given in Table 2.

The wires were cold-drawn in Contours Ltd., Orrville, OH (a member of the Bekaert Group, Kortrijk, Belgium) in one pass under precisely controlled conditions to a final diameter of 18 mm (20% reduction in section). A monoblock machine was used for this purpose. Die geometry is shown in Fig. 1. The main parameters are the following: initial diameter $d_0 = 20.00$ mm, final diameter $d_1 = 17.91$ mm, bearing length $l_z = 6.36$ mm (35.5% d_1), and die inlet angle $2\alpha = 15.36°$.

Residual stresses are very sensitive to any processing after drawing (especially the straightening process). To avoid any change in the residual stress pattern generated by drawing, bars were kept straight during the whole process.

The mechanical properties of drawn wires are shown in

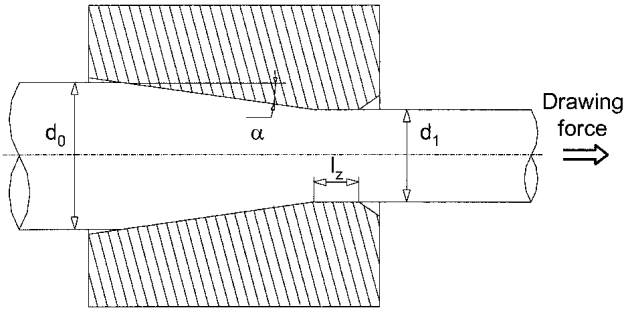

Fig. 1 Die geometry used in the drawing process

Table 1 Chemical Composition of Ferritic and Pearlitic Steel Wires

Wire	C, %	Si, %	Mn, %	P, %	S, %	Al, %
Ferritic	0.04	0.10	0.20-0.45	0.035	0.035	0.02-0.06
Pearlitic	0.78	0.15-0.35	0.60-0.90	<0.025	<0.025	0.02-0.06

Table 2 Mechanical Properties of the Steel Wires Before Drawing

Wire	*E*, GPa	$R_{p0.2}$, MPa	R_m, MPa	ε_{Rm}, %
Ferritic	200	230	340	21.7
Pearlitic	200	515	945	8.6

Table 3 (each value is the average of at least three tests). Comparison between stress-strain curves of the ferritic and pearlitic wires before and after drawing is given in Fig. 2. It can be seen that the drawing process produces a substantial hardening and a clear decrease in ductility, which are most noticeable in the ferritic steel wire.

2.2 Residual Stress Measurement by XRD

Residual stresses were measured at the surface of the wires by XRD.[10,11] The interplanar lattice spacing between the (*hkl*) planes can be calculated using Bragg's law by simply measuring the 2θ angle at which the reflection occurs for a fixed wavelength of the incident flux. From that, the longitudinal strain along the direction of the scattering vector—the bisector between incident and diffracted beam—(L_3 direction in Fig. 3) may be obtained from the formula:

$$(\varepsilon'_{33})_{\phi\psi} = \frac{d_{\phi\psi} - d_0}{d_0} \qquad \text{(Eq 1)}$$

where ε'_{33} is the longitudinal strain along the L_3 direction, $d_{\phi\psi}$ is the lattice spacing for a given combination of ϕ and ψ angles, and d_0 is the unstressed lattice spacing.

For isotropic materials, if the stress tensor in the irradiated layers can be considered biaxial (i.e., the stress components in the direction of the surface normal S_3 are negligible), Eq 1 becomes[19]

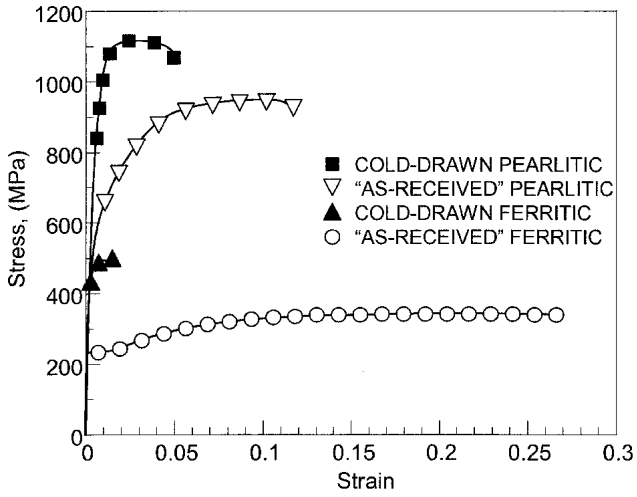

Fig. 2 Comparison between stress-strain curves of the ferritic and pearlitic steel wires before and after drawing

Table 3 Mechanical Properties of the Steel Wires After Drawing

Wire	*E*, GPa	$R_{p0.2}$, MPa	R_m, MPa	ε_{Rm}, %
Ferritic	205	475	500	1.6
pearlitic	192	940	1115	2.2

$$(\varepsilon'_{33})_{\phi\psi} = \frac{d_{\phi\psi} - d_0}{d_0} = \frac{1+\nu}{E}\sigma_\phi \sin^2\psi - \frac{\nu}{E}(\sigma_{11} + \sigma_{22}) \qquad \text{(Eq 2)}$$

where σ_ϕ is the stress component along the S_ϕ direction (Fig. 3). Therefore, σ_ϕ may be obtained directly from the slope of a least-squares line fitted to experimental data, measured at various ψ, if the elastic constants *E* and υ and the unstressed lattice spacing d_0 are known.

In this work, measurements were performed with a Rigaku Strainflex (Tokyo, Japan) analyzer (30 kV and 8 mA). The α-Fe reflection under study was (2,1,1), which produces a Bragg peak at $2\theta = 156.08°$ for the Cr K_α radiation used ($\lambda = 2.2909$ Å). Experiments were performed in Ω-mode. Diffraction peaks corresponding to ten values of ψ angle ($\sin^2\psi$ interval from nearly 0-0.7) were recorded for each residual stress measurement. Parallel beam optics and Soller slits (1°) were used both at the x-ray tube and the scintillation detector to minimize defocusing errors.

The lattice spacing measured at a preliminary diffraction run (at $\psi = 42°$) is substituted for the unstressed lattice spacing d_0 in Eq 2. This is based on the fact that, for most materials, elastic strains may introduce at most a 0.1% difference between the true d_0 and *d* at any ψ.[10] In addition, the single-crystal elastic constants for the (2,1,1) reflection of α-iron are used to calculate *E* and υ.[20]

The above-mentioned method for calculating residual stresses is based upon the assumption of a uniform biaxial stress state within the volume sampled by the x-ray beam. If shear stresses (σ_{12}, σ_{13}) are present, ψ-splitting results (the d versus $\sin^2\psi$ data have opposite curvature for positive and negative ψ). If, in turn, the normal stress σ_{33} has a steep gra-

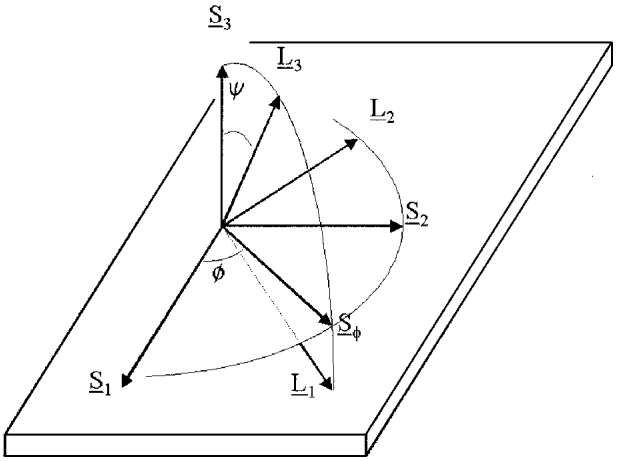

Fig. 3 Definition of the laboratory coordinate system L_i, sample coordinate system S_i, and the angles ϕ,ψ[10]

dient in the surface layers (it must be zero at the surface), curvature occurs in the d versus $\sin^2\psi$ plots and there is no ψ-splitting.[19] In Fig. 4, typical d versus $\sin^2\psi$ plots for ferritic and pearlitic cold-drawn wires are shown for the (2,1,1) α-Fe reflection. It can be seen that the interplanar lattice spacing $d_{2,1,1}$ is a linear function of $\sin^2\psi$ in both wires (the linear correlation coefficient R is close to one in all measurements), in agreement with the hypothesis of a biaxial stress state. So, the residual stress in the ferrite phase can be obtained in both materials from the gradient of the d versus $\sin^2\psi$ plot and Eq 2. In addition, it has been shown[21] by FEM modeling that σ_{33} does not change abruptly with depth (the calculated gradient is about 30 MPa/mm). This means that the maximum value of σ_{33} in the irradiated volume (15 μm depth for the Cr K_α radiation used) would be approximately 5 MPa.

The diffractometer used is a portable system, so all the movements are performed by the goniometer, which includes the x-ray source and detector. With the aim of improving the measurement precision, a special experimental setup was designed for wires. It consists of an XY table (±0.01 mm precision) with two wire supports specially designed for turning the wire around its axis at 45° steps. It allows one to perform measurements in large samples without having to cut them into small pieces. Samples used were 200 mm in length. With this setup, residual stresses can be measured at several cross sections along the same cylinder generatrix or in several generatrices corresponding to the same cross section. In this way, the homogeneity of the surface stress state can be checked.

2.3 XRD Results

Longitudinal residual stresses in the α-Fe phase of the cold-drawn ferritic and pearlitic steel wires were computed at the wire surface by using Eq 2. The experimental results are depicted in Fig. 5 as a function of the distance to the sample edge (measurements were always made along the same generatrix).

In the ferrite phase, the longitudinal residual stress is tensile in both steels. Most of the values range from 200 to 240 MPa for the ferritic steel, and the stress goes to zero very quickly close to the specimen edges (0 and 200 mm, respectively).

The residual stresses in the ferrite phase of the pearlitic steel are lower than in the ferritic steel, with values ranging from

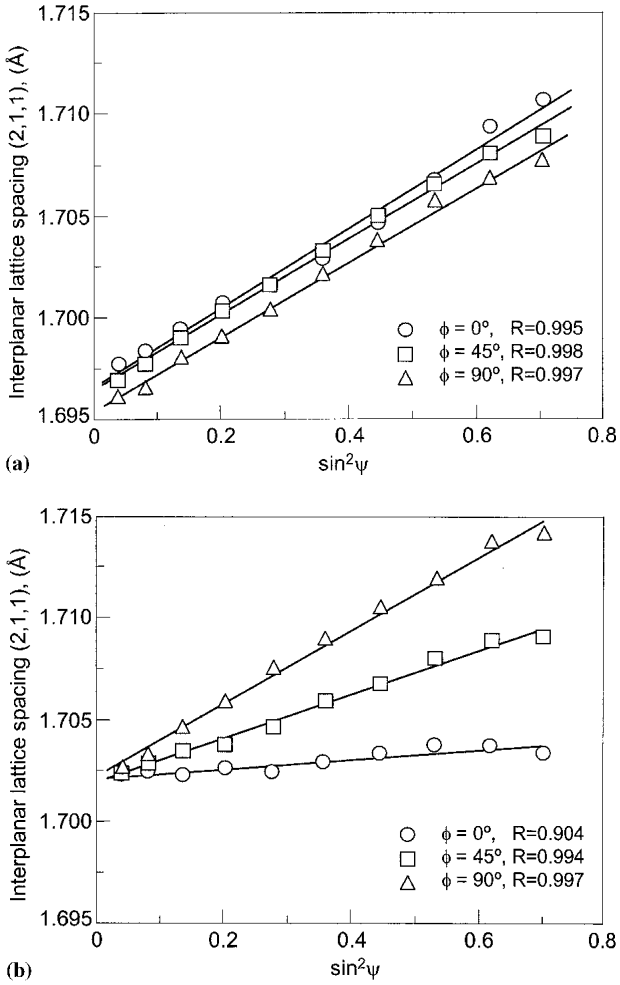

Fig. 4 Interplanar lattice spacing of (2,1,1) planes versus $\sin^2\psi$ for ϕ = 0°, 45°, and 90°: **(a)** cold-drawn ferritic steel wire, and **(b)** cold-drawn pearlitic steel wire. The linear correlation coefficient R for each curve is also enclosed.

approximately 20 to 60 MPa. Measured stresses do not change abruptly with length in the central part of the wire. However, close to the specimen edges, they change to compressive stresses. The effect of the free surface is noticeable within a distance between 20 and 30 mm from the specimen edges.

After measuring the residual stresses, the original samples (200 mm length) were cut in three pieces, as shown in Fig. 6:

- Zone I: 50 mm from left edge
- Zone II: 50 mm from right edge
- Central Zone: the remaining 100 mm in the middle of the sample

After cutting, longitudinal residual stresses were again measured in the three pieces as a function of the edge distance, with the same reference system and along the same generatrix as in the original sample of 200 mm in length. The data corresponding to the ferritic steel are shown in Fig. 7, together with the results before cutting. In the shorter pieces, Zones I and II, the maximum stress almost coincides with the values obtained for the sample before cutting at the same wire location, which

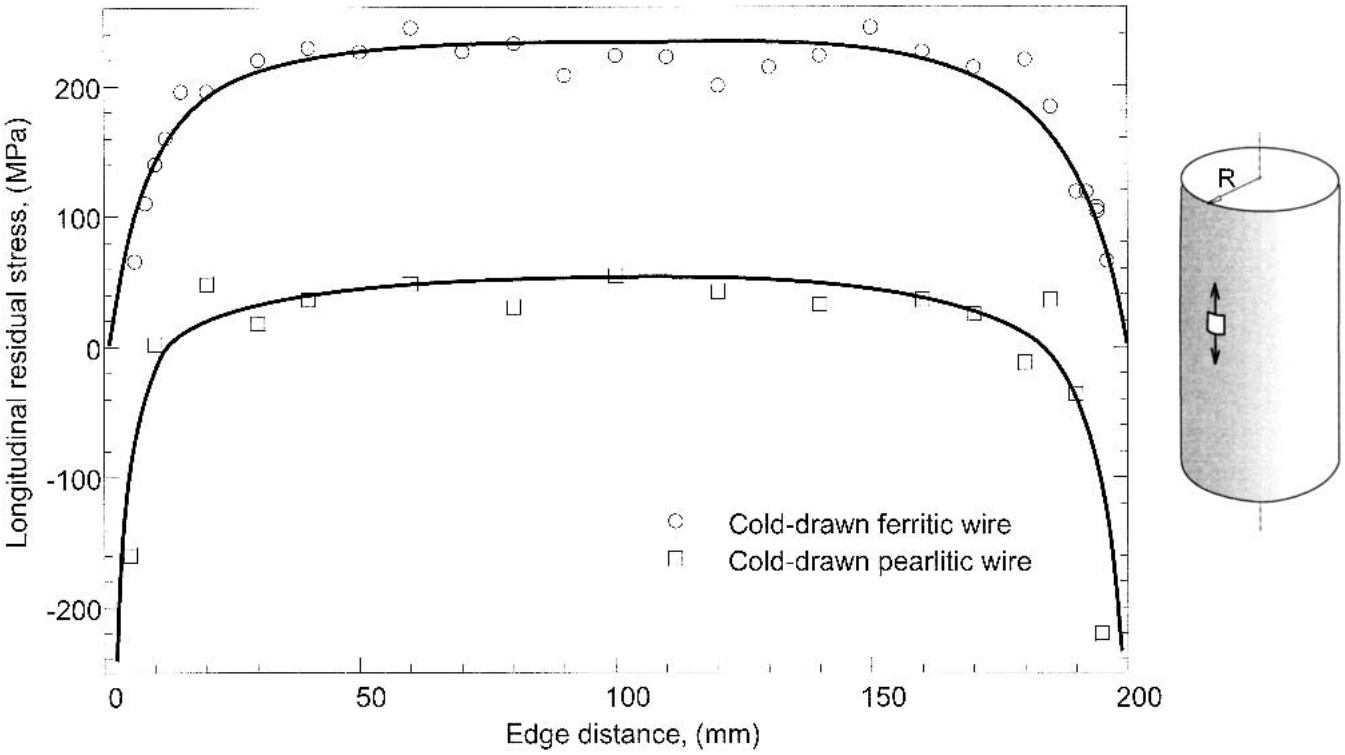

Fig. 5 Surface longitudinal residual stress vs edge distance in the ferrite phase of cold-drawn ferritic and pearlitic steel wire (sample 200 mm long)

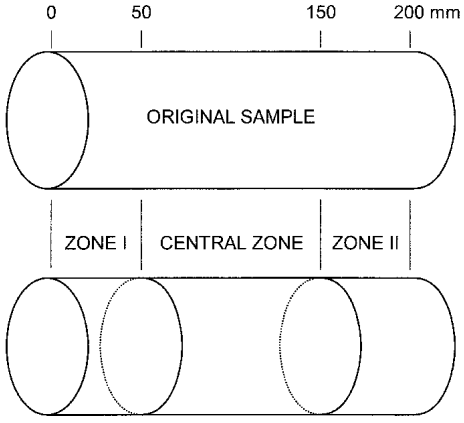

Fig. 6 Sketch of the cutting process

proves the repeatability of the positioning system and the measurement reliability. However, stresses decrease quickly to zero close to the borders of the individual pieces. The same behavior is observed in the longer piece corresponding to the Central Zone. In the Central Zone, it seems that the region influenced by the edges is less than in the shorter pieces corresponding to Zones I and II.

The results obtained in the ferritic phase of the pearlitic steel are shown in Fig. 8. The observed behavior is very similar to that of the ferritic steel. In the shorter pieces, Zones I and II, longitudinal stress grows quickly from around −200 MPa close to the edge to the values corresponding to the sample before cutting at around 20-30 mm from the edge. After that, the stress values remain fairly constant within 5-10 mm and finally decrease quickly below −200 MPa in the final portion of specimen. The same behavior is observed in the longer piece, the Central Zone. The only difference lies in the wire length where the stress reaches a value similar to that of the original sample, which in this case is approximately 50 mm.

3. Numerical Study

3.1 Numerical Model

A numerical model using the code ABAQUS[22] was developed to study residual stresses generated by drawing. It reproduces the passing of the wire through a drawing die. The model takes into account the mechanical and thermal part of the problem but not the influence of phase transformation. Nowadays, modern lubricants and efficient cooling allow the control of wire temperature during the process, so it does not go beyond 250 °C at the surface. Under these conditions, a phase transformation is unlikely to happen in steel.[23]

Residual stresses may appear as an elastic response to a non-uniform distribution of plastic strain. An elastoplastic law with strain hardening was chosen to model the wire behavior (Fig. 9). Isotropic hardening with a von Mises criterion was used, and as a first approximation, the yield locus was considered independent of strain rate. The constitutive equation used as the initial data of the model is the stress-strain curve of the corresponding steel before drawing.

The basic hypothesis of the elastoplastic models is that strain can be divided in two parts: elastic and plastic (Fig.

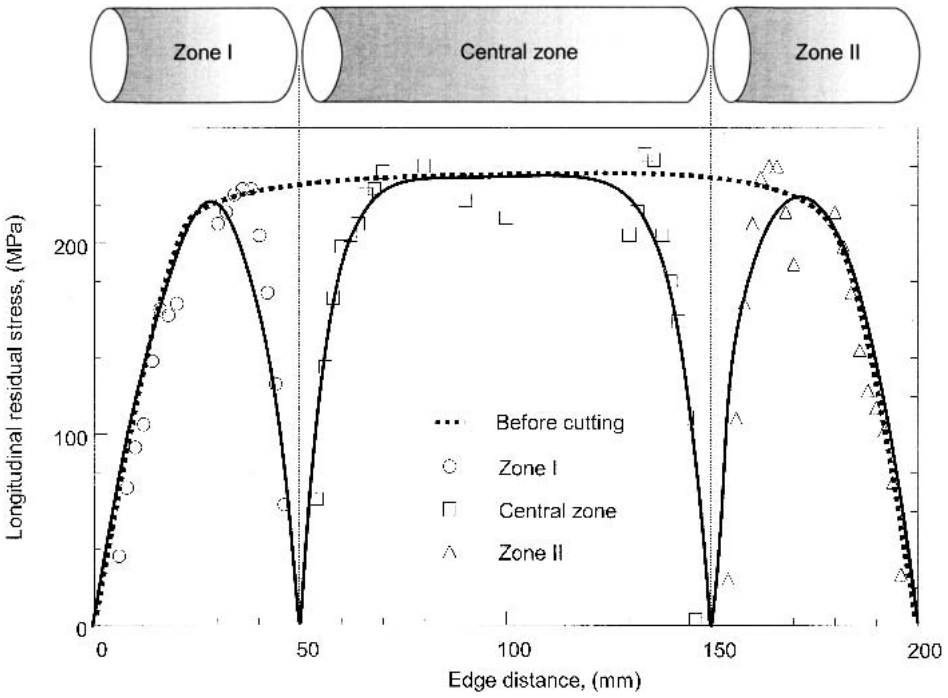

Fig. 7 Surface longitudinal residual stress vs distance to border in cold-drawn ferritic steel wire (before and after cutting)

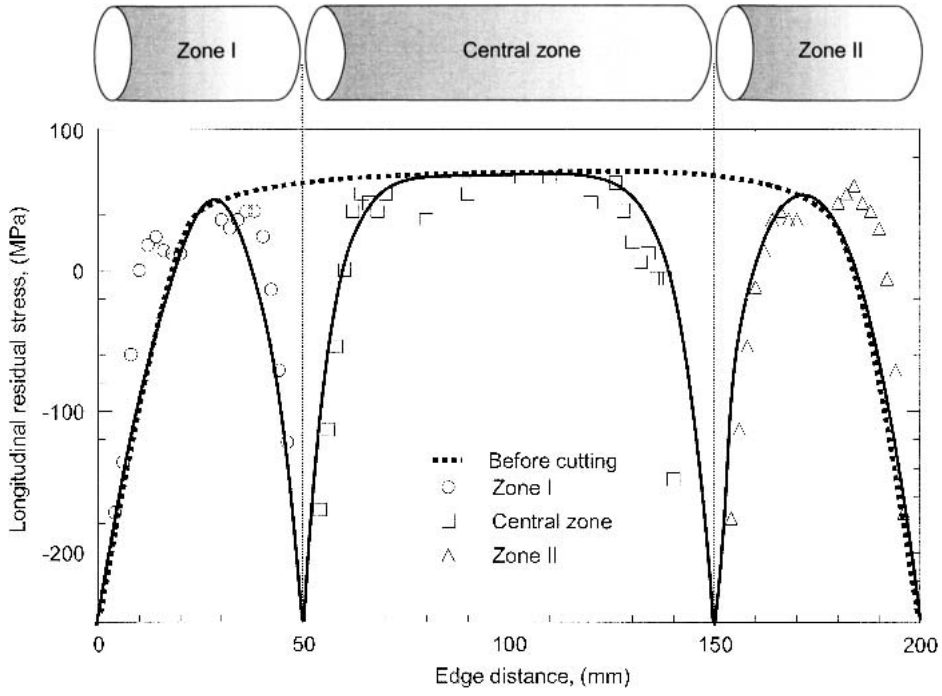

Fig. 8 Surface longitudinal residual stress vs distance to border in the ferrite phase of cold-drawn pearlitic steel wire (before and after cutting)

9).[24] Plastic response was considered incompressible, and three different kinds of elements (8-nodes with reduced integration, 8-nodes with incompatible modes of deformation, and 8-nodes hybrid) were used to avoid the problem of volumetric locking.[24-26] The results from the simulation were almost the same for the three kinds of elements.

3.1.1 Drawing Simulation. The drawing process has been simulated by making the wire pass through the die. To this end, the displacement of the front end of the wire was imposed. That is a realistic approach because in the real process the wire is forced to pass through the die by pulling it from the point.

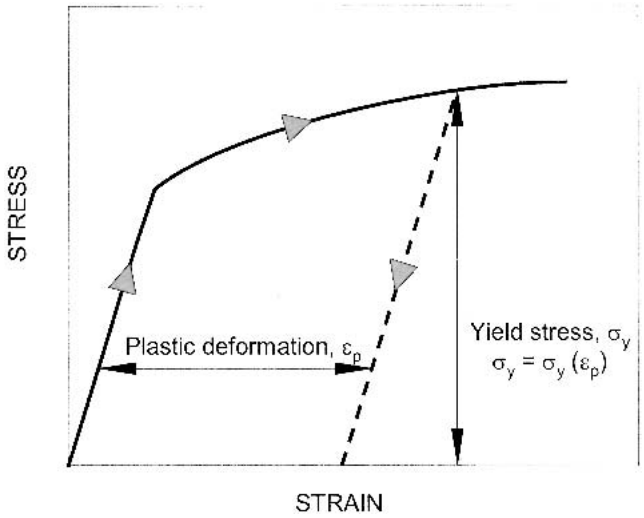

Fig. 9 Elastoplastic law used to model the wire mechanical behavior

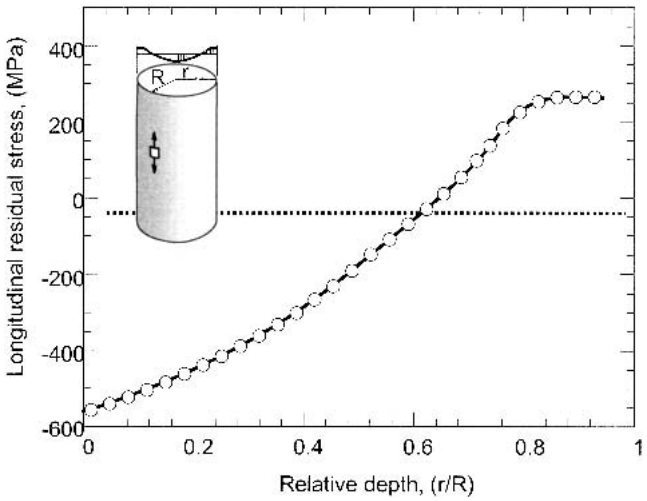

Fig. 10 Longitudinal residual stress as a function of relative depth (*r/R*) in the ferritic steel wire after drawing (FEM simulation)

The die (see Section 2.1 and Fig. 1) was modeled as an elastic material (elastic modulus of tungsten carbide). The contact between the wire and the die has been reproduced with a Coulomb friction coefficient, which ranges from 0.01 to 0.2 in industrial practice. Calculated stresses were almost the same within this range.[21]

Residual stresses are calculated at the end of the process, when the whole wire has passed through the die, in a zone where the stationary state has been reached. Starting and final parts of the wire are not considered for this purpose.

3.1.2 Cutting Simulation. The cutting process described in Section 2.3 (Fig. 6) was numerically simulated to study the effect of the new surfaces on existing residual stresses. The simulation was performed in three steps:

1) First, a number of model elements were removed from the original wire (after passing through the die) until the required length (100 mm for central zone or 50 mm for Zones I and II) was attained.
2) Second, a stress state equal and opposite to the residual stress state of the wire before cutting was applied to the new free surfaces, so as to achieve the equilibrium condition.
3) Finally, residual stresses with the new boundary conditions were calculated.

3.2 Results

3.2.1 Ferritic Wire. The longitudinal residual stress profile of the ferritic wire after drawing is shown in Fig. 10. Stresses were calculated along one diameter and plotted as a function of relative depth *r/R*, where *r* is the distance from the wire center and *R* is the wire radius. The self-equilibrium condition is verified in the wire section. It can be observed from Fig. 10 that the stresses are tensile at the surface and compressive at the wire core, with values ranging from 250 MPa to −550 MPa, respectively.

Figure 11 represents the effect of the simulated cutting process on the calculated longitudinal residual stresses at the wire surface. In all three pieces (Zones I and II and Central Zone of Fig. 6) the stress grows from zero at the wire edges to approximately 220 MPa—the residual stress value before cutting—at the central part of each piece. The shorter the wire, the more noticeable the region influenced by the new free surfaces created by cutting as compared with the total length. It can be seen that stresses reach realistic values at a distance of about 20-30 mm from the wire edges.

3.2.2 Pearlitic Wire. The residual stress profile calculated for the pearlitic wire is shown in Fig. 12. There, longitudinal residual stresses are plotted as a function of the relative depth *r/R*. As happened with the ferritic wire, residual stresses are tensile at the surface and compressive at the wire core, with values ranging from 400 to −800 MPa, respectively. As happened with the ferritic wire, the calculated stress profile also fulfils the self-equilibrium condition.

When the simulation of the cutting process is carried out with the pearlitic wire, the results of Fig. 13 are obtained. Close to the specimen edges, irrespective of the sample length, the stress goes to zero very quickly. At the central part of each piece the stress reaches a value around 400 MPa, which is very similar to the one calculated before cutting. The region where the stress values become affected by the free surface boundary condition measures approximately 20 mm. As occurred with the ferritic wire, in the shorter samples (Zones I and II), this leaves very little area in which the stresses are representative of the values before cutting.

4. Discussion

4.1 Ferritic Wire

Experimental and numerical results show that the cold-drawing process suffered by the ferritic wire generates noticeable tensile residual stresses at the surface, with the maximum value being about 45% of the tensile strength. The residual stress profile calculated by FEM matches very well with the experimental measurements by XRD at the wire surface. From Fig. 5, it can be seen that most longitudinal residual stresses measured at the surface are located in a scatter band of about 40 MPa (between 200 and 240 MPa), whereas the numerical

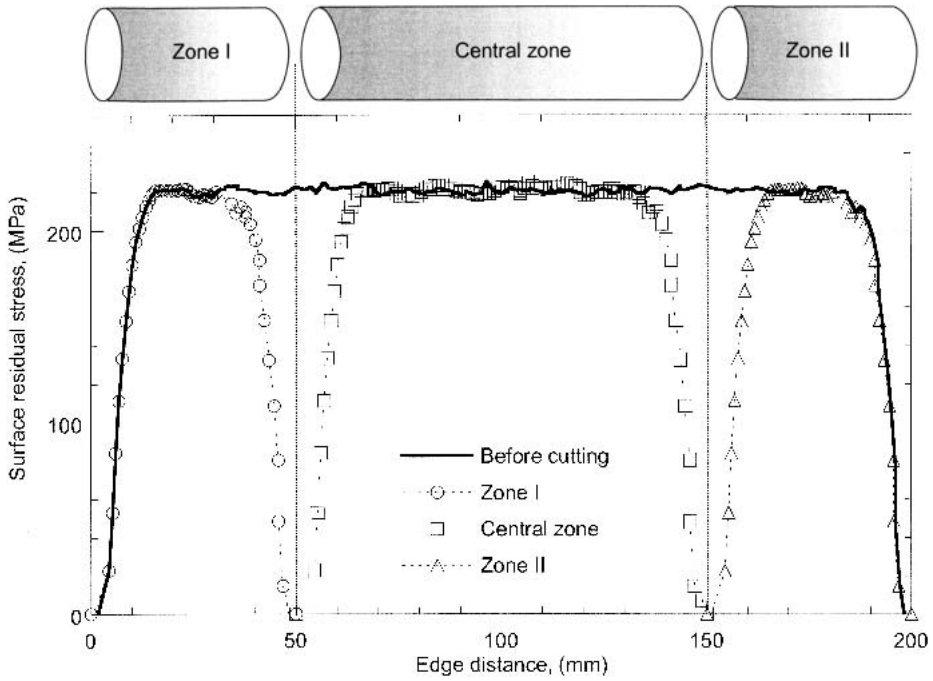

Fig. 11 Surface longitudinal residual stresses calculated by FEM vs distance to the border in cold-drawn ferritic steel wire (before and after cutting)

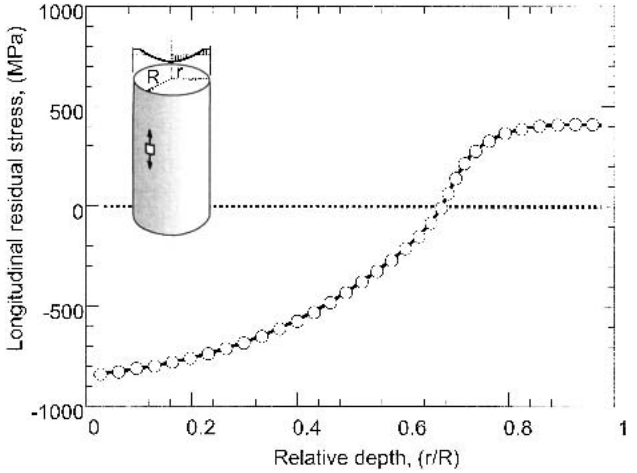

Fig. 12 Longitudinal residual stress as a function of relative depth (*r/R*) in the pearlitic steel wire after drawing (FEM simulation)

simulation gives values close to 220 MPa at the wire surface (see Fig. 11).

Wire drawing is an axisymmetric process, so a uniform residual stress state all along the surface of the wire is expected. X-ray measurements performed in a given cross section along several generatrices have confirmed this fact. However, it has been observed that local defects may cause important changes on the stress values. Therefore, valuable information about residual stress state may not be inferred from a few measurements. Instead, many points have to be sampled in several cross sections to get relevant results.

The cutting process is adequately simulated by FEM, as shown in Fig. 14. Experimental measurements and numerical calculations point out that the region where the stresses are affected by the free surface ranges from 20 to 30 mm in length (between 1 and 1.5 times the wire diameter). This means that in the case of the 50 mm specimen (Fig. 14c), surface residual stress measurements are not representative of the actual stress state generated by cold drawing.

4.2 Pearlitic Wire

In multiphase materials, XRD must be carried out in each of the constituent phases to obtain the total residual stress. However, sometimes this is not possible, as happens in our case. Wires used for pre-stressed concrete have a fully pearlitic microstructure composed of nano-sized alternating ferrite and cementite lamellae. Diffraction peaks from the cementite phase cannot be easily obtained with commercial x-ray diffractometers, for the volume fraction of cementite in pearlite is very low (around 12%). Therefore, residual stress measurements by XRD give information only about stresses in the ferrite phase.

Longitudinal residual stresses measured by XRD in the ferrite phase of the pearlitic steel are fairly homogeneous along the wire length. Stress values range from 20 to 60 MPa in the central zone of the wire and decrease very quickly when the specimen edges are approached (Fig. 5). However, unlike the ferritic steel, residual stresses close to the free surfaces are not zero, but negative. The explanation lies in the fact that with XRD we are obtaining information about only the residual stresses in the ferrite phase of a two-phase material. We do not know how much stress is carried out by the cementite phase. If we take into account that ferrite represents around 88% in volume of pearlite and we apply the equilibrium condition between phases, the total residual stress σ^T would be:

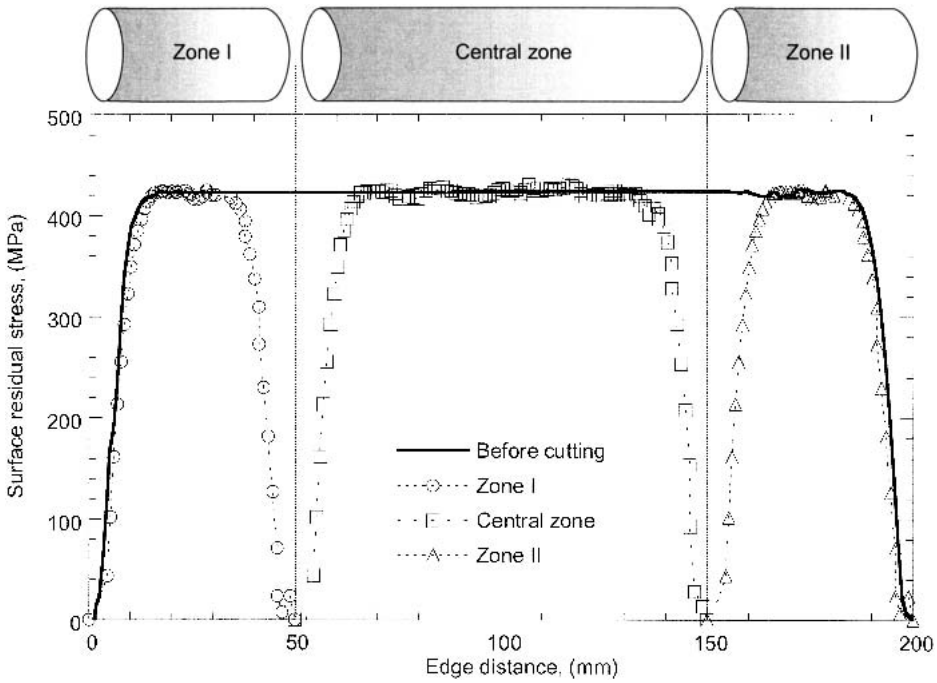

Fig. 13 Surface longitudinal residual stresses calculated by FEM vs distance to the border in cold-drawn pearlitic steel wire (before and after cutting)

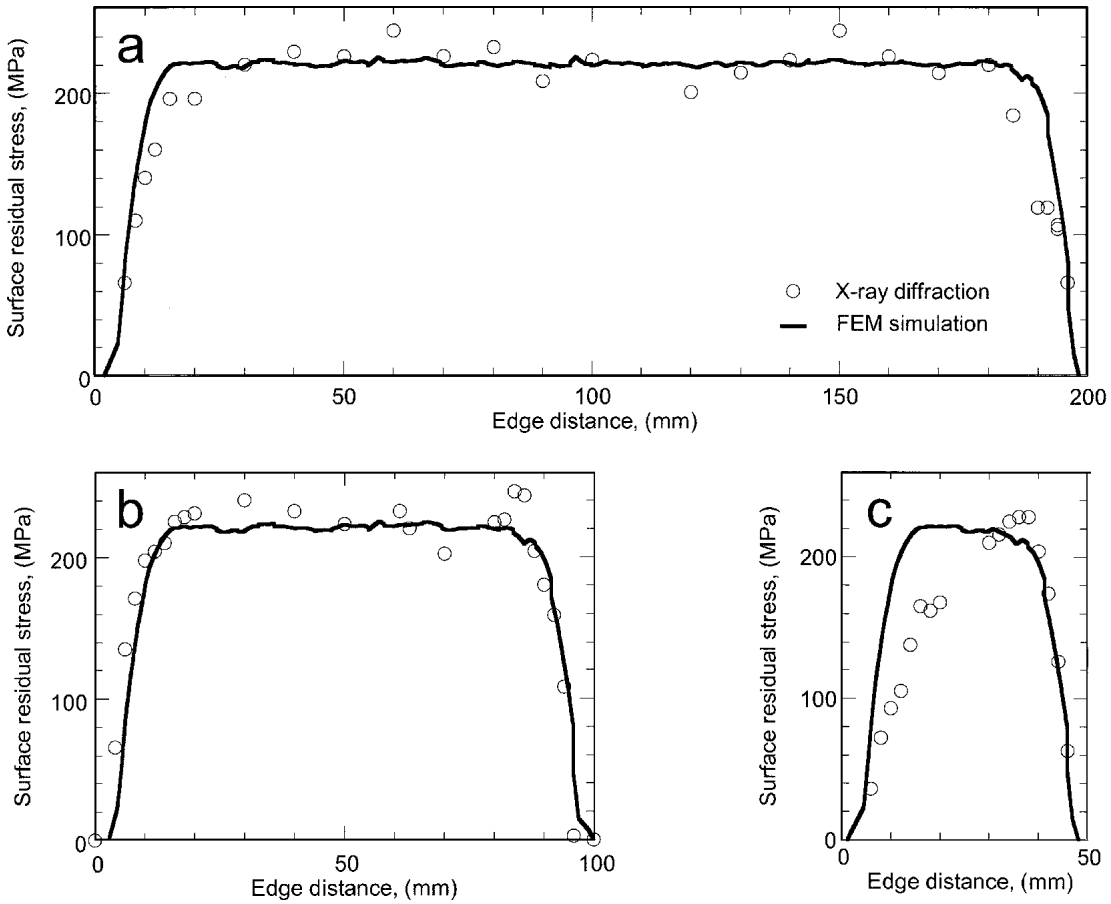

Fig. 14 Comparison between XRD measurements and FEM simulations of longitudinal residual stresses at the surface of the ferritic steel wire: **(a)** before cutting (200 mm specimen), **(b)** and **(c)** after cutting (100 and 50 mm specimens, respectively)

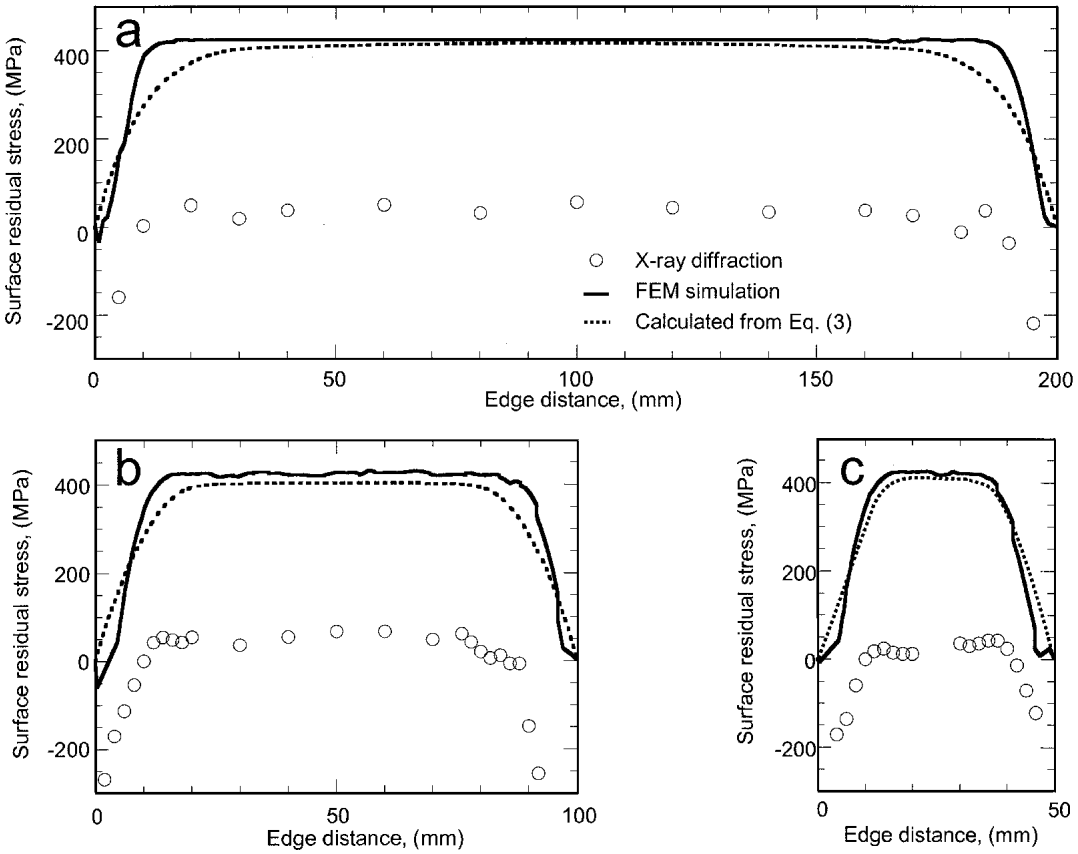

Fig. 15 Comparison between XRD measurements (stresses in ferrite phase), FEM simulations (total stresses), and calculations from Eq 3 of longitudinal residual stresses at the surface of the pearlitic steel wire: **(a)** before cutting (200 mm specimen), **(b)** and **(c)** after cutting (100 and 50 mm specimens, respectively).

$$\sigma^T = V_f \sigma^f + V_c \sigma^c \quad \text{(Eq 3)}$$

where V_f and V_c are the volume fractions of ferrite and cementite in pearlite (88% and 12%, respectively), and σ^f and σ^c are the corresponding residual stresses in both phases. At a free surface, total stresses must vanish. From Fig. 5 and 8, the longitudinal stress carried out by the ferrite phase at the wire edge is around −250 MPa. The corresponding residual stress in cementite can be estimated by applying the free surface boundary condition to Eq 3. The resulting stress is then around 1800 MPa.

Numerical simulation of the drawing process gives information on the total residual stress developed in the material. In the single-phase ferritic wire, total stress coincides with ferrite phase stress measured by XRD. However, in the case of the pearlitic wire, numerical results cannot be compared with residual stresses measured by XRD, because the latter only provide values for the ferrite phase. If the cementite phase stress calculated above at the wire edge is used in conjunction with Eq 3, the total residual stress at any point of the wire surface can be estimated. Far from the specimen edges, the measured residual stress in the ferrite phase averages 40 MPa, an increase of around 300 MPa from the wire edge value (Fig. 5). On the other hand, the total residual stress predicted by FEM simulation is increased from zero at the wire edges to around 400 MPa at the central part of the specimen (Fig. 13). The increase in the cementite phase stress can be calculated from Eq 3:

$$\Delta\sigma^T = V_f \Delta\sigma^f + V_c \Delta\sigma^c \quad \text{(Eq 4)}$$

where $\Delta\sigma^T$, $\Delta\sigma^f$, and $\Delta\sigma^c$ are the increments in the total, ferrite, and cementite stress, respectively. The resulting increment in the cementite phase stress from the wire edge data is around 1200 MPa. Therefore, the cementite stress at a point of the wire surface far from the wire edges is approximately 3000 MPa. The values obtained for the cementite stress agree with the published data.[11,27,28]

The FEM simulation of the cutting process yields total residual stresses at the wire surface, which are considerably higher than the XRD measurements on the ferrite phase (Fig. 5 and 13). In Fig. 15, a comparison is given between XRD measurements (stress in the ferrite phase), FEM simulations, and calculations from Eq 3. It can be seen that the total stresses calculated from Eq 3 give values very close to the FEM simulations; the residual stress at the wire edges being zero in both cases, in agreement with the free surface boundary condition. As happened with the ferritic wire, the extension of the region affected by the free surface is again similar to the wire diameter.

5. Conclusions

The cutting of specimens affects residual stresses in a length between 1 and 1.5 times the wire diameter, so to know the actual residual stresses it is recommended that specimens larger than 5 times the diameter are used, to have a central region (about three diameters) free from the perturbations created by cutting.

In spite of the above-mentioned data, in many diffractometers used for residual stress measurements, geometry and sample holder limitations make it necessary to use very small samples. The results from the current study may serve as a warning for measurements obtained in such conditions. Residual stress values obtained in a small sample might not be representative of the actual stress state. However, in multiphase materials, residual stress measurements close to the free surfaces may yield useful information on stress partitioning between phases.

Acknowledgements

The authors are indebted to Mr. Javier del Río, from Bekaert, for providing the material. They also want to thank Dr. Federico Mompeán, Dr. Mar García, and Mrs. María Martínez for useful discussions about cementite stresses. Funding from the Spanish Government through FEDER UNPM00-33-003 and FEDER UNPM00-33-004, and research projects 2FD97-1513 and MAT2002-04343 is gratefully acknowledged.

References

1. CUR: "Cases of Damage to Corrosion of Prestressing Steel," Netherlands Committee for Concrete Research, Report 49, The Hague, The Netherlands, 1971.
2. E. Philips: "Survey of Corrosion of Prestressing Concrete Water-Retaining Structures," Australian Water Resources Council, Paper 9, Canberra, Australia, 1975.
3. M. Elices, G. Maeder, and V. Sánchez-Gálvez: "Effect of Surface Residual Stress on Hydrogen Embrittlement of Prestressing Steels," *Brit. Corr. J.*, 1983, *18,* pp. 80-81.
4. J. LLorca and V. Sánchez-Gálvez: "Fatigue Limit and Fatigue Life Prediction in High Strength Cold Drawn Eutectoid Steel Wires," *Fatigue Frac. Eng. M.*, 1989, *12,* pp. 31-45.
5. J. LLorca and V. Sánchez-Gálvez: "Numerical Determination of the Influence of Residual Stresses on Fatigue" in *Computational Plasticity*, D.R.J. Owen, E. Hinton and E. Oñate ed., Pineridge Press, Swansea, UK, 1987, pp. 1123-36.
6. P.J. Webster and G. Mills: "Residual Stresses in a Steel Strand," *Physica B*, 1997, *241-243,* pp. 1270-73.
7. K. Katagiri, T. Sato, K. Kasaba, S. Sasaki, and H. Tashiro: "Effects of Post-Drawing Treatments on the Fatigue Strength of Eutectoid Steel Wires," *Fatigue Frac. Eng. M.*, 1999, *22,* pp. 753-60.
8. S. Beretta and M. Boniardi: "Fatigue Strength and Surface Quality of Eutectoid Steel Wires," *Int. J. Fatigue*, 1999, *21,* pp. 329-35.
9. A. Ben Rhouma, C. Braham, M.E. Fitzpatrick, J. Lédion, and H. Sidhom: "Effects of Surface Preparation on Pitting Resistance, Residual Stress, and Stress Corrosion Cracking in Austenitic Stainless Steels," *J. Mater. Eng. Perform.*, 2001, *10*(5), pp. 507-14.
10. I.C. Noyan and J.B. Cohen: *Residual Stress: Measurement by Diffraction and Interpretation*, Springer-Verlag, New York, NY, 1987.
11. K. Van Acker: "Inwendige Spanningen in Koudvervordme Metalen en in Metaalmatrixcomposieten," Ph.D. Thesis, K.U. Leuven, Belgium, 1996 (in English).
12. V. Hauk and E. Macherauch: "A Useful Guide for X-Ray Stress Evaluation," *Adv. X Ray Anal*., 1984, *27,* pp. 81-99.
13. K. Masubushi: *Analysis of Welded Structures. Residual Stress and Distortion and Their Consequences*, Pergamon Press, Oxford-New York, 1980.
14. J. Peters, R. Snoeys and M. Mars: "Residual Stress in Grinding" in *Advanced Fabrication Processes*, Proc. Agard, Conference Proceedings, Neuilly Sur Seine, France, 1978, *256,* pp. 2.1-2.15.
15. E. Schneider and K. Goebbles: "Determination of Mechanical Stress by Polarized Shear Waves" in *New Procedures in NDT*, P. Holler ed., Springer Verlag, Berlin, Germany, 1983, pp. 551-60.
16. B. Sundström and K. Törrönen: "The Use of Barkhausen Noise Analysis in Nondestructive Testing," *Mater. Eval.*, 1979, *2,* pp. 51-56.
17. S. Sharma, H. Mao, P. Bell and J. Xu: "Measurement of Stress in Diamond Anvils With Micro Raman Spectroscopy," *J. Raman Spectrosc.*, 1985, *16*(5), pp. 350-51.
18. S. Carlsson and P.L. Larsson: "On the Determination of Residual Stress and Strain Fields by Sharp Indentation Testing. Part I: Theoretical and Numerical Analysis," *Acta Mater.*, 2001, *49,* pp. 3179-91.
19. I.C. Noyan: "Effect of Gradients in Multi-Axial Stress States on Residual Stress Measurements With X-Rays," *Metall. Trans. A*, 1983, *14A,* pp. 249-58.
20. R.W. Hertzberg, *Deformation and Fracture Mechanics of Engineering Materials*, 9th ed., John Wiley and Sons, New York, 1996, pp. 10-16.
21. J.M. Atienza: "Tensiones Residuales en Alambres de Acero Trefilados," Ph.D. Thesis, Universidad Politécnica de Madrid, Spain, 2001 (in Spanish).
22. Hibbitt, Karlsson, and Sorensen Inc.: *ABAQUS Manual*, version 5.8, Pawtucket, RI, 1998.
23. T. Hamada, T. Hirouchi, and M. Akiyama: "A Numerical Study of Temperature in a Fine High Carbon Steel Wire Subjected to High Speed Drawing," *Wire J. Int.*, 2001, *34*(5), pp. 86-92.
24. O.C. Zienkiewicz and R.L. Taylor, *The Finite Element Method*, 9th ed., McGraw-Hill, London, UK, 1989.
25. A.J.L. Crook and E. Hinton: "Comparison of 2d Quadrilateral Finite Elements for Plasticity Problems" in *Computational Plasticity*, D.R.J. Owen, E. Hinton and E. Oñate, ed., Pineridge Press, Swansea, UK, 1989, pp. 181-95.
26. K.J. Bathe, M. Kojic, and J. Walczak: "Developments in Methods for Large Strain Elasto-Plastic Problems" in *Computational Plasticity*, D.R.J. Owen, E. Hinton and E. Oñate, ed., Pineridge Press, Swansea, UK, 1989, pp. 263-75.
27. K. Van Acker, J. Root, P. Van Houtte, and E. Aernoudt: "Neutron Diffraction Measurement of the Residual Stress in the Cementite and Ferrite Phases of Cold Drawn Steel Wires," *Acta Metall. Mater.*, 1996, *44,* pp. 4039-49.
28. Y. Tomota, P. Lukás, D. Neov, S. Harjo, and Y.R. Abe: "In Situ Neutron Diffraction During Tensile Deformation of a Ferrite-Cementite Steel," *Acta Mater.*, 2003, *51*(3), pp. 805-17.